Investigation of Acetic Acid Hydration Shell Formation through Raman Spectra Line-Shape Analysis

ARTICLE *in* THE JOURNAL OF PHYSICAL CHEMISTRY B · OCTOBER 2012

Impact Factor: 3.3 · DOI: 10.1021/jp3088594

6 AUTHORS, INCLUDING:

Francesco D'Amico
Sincrotrone Trieste S.C.p.A.
34 PUBLICATIONS **207** CITATIONS
SEE PROFILE

Filippo Bencivenga
Sincrotrone Trieste S.C.p.A.
63 PUBLICATIONS **386** CITATIONS
SEE PROFILE

Riccardo Cucini
Italian National Research Council
40 PUBLICATIONS **189** CITATIONS
SEE PROFILE

Claudio Masciovecchio
Sincrotrone Trieste S.C.p.A.
149 PUBLICATIONS **2,810** CITATIONS
SEE PROFILE

THE JOURNAL OF PHYSICAL CHEMISTRY B

Article

pubs.acs.org/JPCB

Investigation of Acetic Acid Hydration Shell Formation through Raman Spectra Line-Shape Analysis

Francesco D'Amico,* Filippo Bencivenga, Alessandro Gessini, Emiliano Principi, Riccardo Cucini, and Claudio Masciovecchio

Sincrotrone Trieste, Strada Statale 14 km 163.5, Area Science Park, I-34012 Trieste, Italy

ABSTRACT: Raman spectra of acetic acid aqueous solutions in the 500−4000 cm^{-1} range have been measured as a function of water concentration to investigate the hydration shell formation mechanism around the acetic acid molecules. A fitting procedure based on the Kubo−Anderson model has been applied to the spectra. This has allowed us to determine the average lifetime of the hydrogen bonds involving a given functional group, as well as their geometrical distribution as a function of water concentration. The comparison of our results with literature data has demonstrated that the fitting model is adequate to describe organic water mixtures. Finally, the role of water in the formation of the hydrophobic shell around the methyl group in diluted acetic acid water solutions has been discussed, evidencing how the methyl group hydrophobicity strongly influences the acetic acid behavior in aqueous solutions.

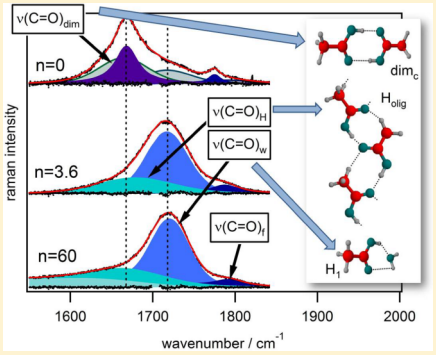

INTRODUCTION

Hydrogen bonds (HB) play a fundamental role in the chemistry of the life:[1−3] protein folding mechanisms, catalysis, and many other biochemical behaviors arise from HB making and breaking dynamics.[1,4,5] The role of water in determining the behavior of proteins and macromolecules in physiological conditions is still a matter of interest, and despite many decades of intense studies (theoretical and experimental), several contrasting results clearly underline how a comprehensive understanding of the interaction mechanisms between water and biomolecules is still lacking.[6−11]

Among various experimental techniques able to provide information on aqueous solutions of biological molecules, Raman spectroscopy is one of the most widely used.[12−14] The reasons are manifold, e.g.: (i) Differently from infrared absorption, the Raman cross section of water is sufficiently weak to allow investigating also very diluted solutions.[13,14] (ii) Raman peaks in the 500−4000 cm^{-1} range allow us to identify the vibrational modes of each atomic group and, therefore, to discriminate the contributions of single functional groups to the behavior of the whole system;[12] additional information on this aspect could be added by resonant and/or polarization-resolved Raman spectroscopy.[13−15] (iii) The Raman spectra line shape depends both from specific intramolecular interactions and from the interactions between the vibrating atoms and the surrounding environment.[15,16] From Raman data it is then possible to extract information both on the behavior of the single parts of a molecule with respect to the whole system and on the local (intermolecular) environment.

Despite this large potentiality, several Raman studies on biosystems are merely based on empirical comparisons aimed at characterizing the behavior of basic features such as, e.g., the shift in the center of mass of the peak.[17−22] On one hand, such an approach is robust because it does not rely upon any underlying theoretical or phenomenological frame. However, on the other hand, it often fails in providing an exhaustive characterization of the system; indeed, to provide reliable results, auxiliary data obtained from other experimental techniques or numerical simulations are frequently used.[19,21−25] More in general, a proper line shape analysis of Raman spectra always allows us to retrieve additional information that are otherwise lost.

The isotropic Raman spectrum ($I_{iso}(\omega)$) can be expressed as the Fourier transform of the vibrational correlation function $\langle q_v(0)\, q_v(t)\rangle_{vib}$,[26,27] whereas it can be experimentally determined by performing polarized and depolarized Raman scattering experiment;[15,26,27] more specifically

$$I_{iso}(\omega) = \frac{I_{||}(\omega) - \frac{4}{3}I_{\perp}(\omega)}{\int_{-\infty}^{\infty}\left[I_{||}(\omega) - \frac{4}{3}I_{\perp}(\omega)\right] d\omega} \propto \int_0^{\infty} \langle q_v(0)\, q_v(t)\rangle_{vib} e^{i\omega t}\, dt \quad (1)$$

where $I_{||}(\omega)$ and $I_{\perp}(\omega)$ are the Raman spectra collected with the incident beam polarization perpendicular and parallel to the one of the scattered beam.

In the liquid phase, where the Raman line shape principally depends from intermolecular interactions, the Kubo−Anderson model can be used to describe $I_{iso}(\omega)$.[26,28−33] The basic assumptions at the base of the Kubo−Anderson model are (i) the energy levels of atomic oscillations are wavenumber shifted by a stochastic perturbation Hamiltonian, which couples the

Received: September 6, 2012
Revised: October 12, 2012
Published: October 19, 2012

oscillator to the molecular environment and (ii) the correlation function of the frequency displacement ($\omega_I(t)$) is assumed to be exponential,[26,28,29] i.e.:

$$\chi(t) = \frac{\langle \omega_I(t)\, \omega_I(0)\rangle}{\langle [\omega_I(0)]^2\rangle} = \exp\left(-\frac{t}{\tau_c}\right) \tag{2}$$

Within these assumptions the root-mean-square wavenumber displacement of the instantaneous transition wavenumber is given by the vibrational second spectra moment of the band contour:

$$\langle \omega^2\rangle = \frac{\int_{-\infty}^{\infty} I_{\mathrm{vib}}(\omega)(\omega - \omega_I^0)^2\, \mathrm{d}\omega}{\int_{-\infty}^{\infty} I_{\mathrm{vib}}(\omega)\, \mathrm{d}\omega} \tag{3}$$

where ω_I^0 is the unperturbed vibrational frequency. Within this frame, it can be shown that the vibrational correlation function[28,29] can be written as

$$\frac{\langle q_v(0)\, q_v(t)\rangle}{\langle |q_v(0)|^2\rangle} = C(t,\langle\omega^2\rangle, \tau_c) = \exp\{-\langle\omega^2\rangle[\tau_c t - \tau_c^2(1 - \mathrm{e}^{-t/\tau_c})]\} \tag{4}$$

From the above equations it follows[28,29] that

$$I_{\mathrm{iso}}(\omega) \propto \frac{\mathrm{e}^{\alpha^2}}{\alpha} \sum_{n=0}^{\infty} \frac{(-\alpha^2)}{n!} \frac{\alpha + n/\alpha}{(\alpha + n/\alpha)^2 + \frac{(\omega - \omega_0)^2}{\langle\omega^2\rangle}} \tag{5}$$

where $\alpha = (\langle\omega^2\rangle)^{1/2}\tau_c$. Equation 5 can be therefore used to describe the isotropic Raman intensity of a single vibration feature.[30−33] The α parameter determines the speed with which $\chi(t)$ decays on account of the fluctuating intermolecular potentials of the lattice.[26] In the limit of $\alpha \gg 1$ (slow modulation), the initial phase coherence of the individual oscillator is rapidly lost and the perturbation remains significant for a long time, it means that the initial Gaussian spread is the predominant part of the peak, which assumes a Gaussian line shape of width $(\langle\omega^2\rangle)^{1/2}$. Instead, in the $\alpha < < 1$ limit (fast modulation) the effects of the perturbations decrease rapidly and the original phase is remembered for a longer time. It occurs because the spread of the peak, due to the initial Gaussian width, is negligible with respect to the spread due to τ_c. In the latter limit, eq 5 can be approximated by a Lorentzian.[26,30] Moreover, in the fast modulation limit τ_c can be related to the dephasing time τ_{deph} through the following equation:[26]

$$\tau_{\mathrm{deph}} = \frac{1}{\langle\omega^2\rangle\tau_c} \simeq \frac{1}{\pi\Gamma_L} \tag{6}$$

where Γ_L is the Lorentzian width and the inverse of the dephasing time represent the collision rate of the liquid molecules on the vibrating groups.

The main interactions in organic aqueous solutions arise from the continuous making and breaking of HB involving bulk water, hydration water, and solute molecules. Therefore, in the presence of HB involving the vibrating atoms, we can reasonably assume that τ_c is related to HB dynamics, whereas $\langle\omega^2\rangle$ may provide information on the local environment around the functional group(s) involved in the HB (such as, e.g., the degree of local structural disorder). The information coming from such a Raman line shape analysis can then be used instead of or in addition to the simple empirical analysis of spectral features.

To verify the correctness of the above statement, a Raman spectra analysis procedure, based on the Kubo−Anderson model, has been used to analyze Raman spectra from acetic acid aqueous solutions at different concentrations. The choice of the sample basically arises from its molecular simplicity and from the presence of a wide scientific literature.[23−25,34−36] This allowed us to verify that the obtained results are in agreement with the more recent experimental and theoretical studies.[24,35] Finally, the performed line shape analysis also allowed us to clarify some aspects of the acetic acid structural conformations in aqueous solutions, which are still subject of debate.[23−25,34,35]

EXPERIMENTAL SECTION

Solutions were prepared using ultrapure acetic acid (99.7%, Sigma-Aldrich) diluted in bidistilled water. Samples were placed in a 2 mL UV-grade quartz cell. The temperature of the sample was kept fixed at 20 °C. Concentration of water was varied from 0 to 1000 water molecules per acetic acid molecule.

Raman spectra were collected in a backscattering geometry. The radiation source was a 244 nm line of a 10 mW Ar^+ laser, linearly polarized. By using polarizers and wave plates, we collected the relative scattered intensities of both $I_{\parallel}$ and $I_{\perp}$.

The spectrum of scattered light was recorded by a high resolved Raman spectrometer, equipped with three subsequent dispersive stages based on blazed UV-grating of 3600 lines/mm; the photon detector was a nitrogen cooled CCD camera, and the overall spectral resolution was 1 cm^{-1}.

Three wavenumber ranges have been chosen to determine the most relevant acetic acid vibrational frequencies. The first (840−940 cm^{-1}) corresponds to the vibrational stretching between the two carbon atoms of acetic acid, whereas the second and third ranges (1600−1850 and 2900−3000 cm^{-1}) correspond to the C═O and C−H vibrational stretching modes, respectively.[23,25,34] For the sake of simplicity in the following, we will refer to these vibrational modes to as ν(C—C), ν(C═O), and ν(C—H), respectively.

Spectra have been analyzed using a standard fitting procedure based on a χ^2 minimization:

$$\chi^2 = \sum_{k=1}^{J} [y_k - I_{\mathrm{iso}}(\omega_k)]^2 \tag{7}$$

where J = 400−600 indicates the number of channels (wavenumbers) used to sample the Raman spectrum, y_k are the counts recorded by the CCD in that channel, and $I_{\mathrm{iso}}(\omega) = I_{\parallel}(\omega) - (4/3)I_{\perp}(\omega)$ represents the function describing the spectra line shape:

$$I_{\mathrm{iso}}(\omega) = \sum_{i=1}^{N} A_i K_i(\omega,\omega_0^i,\langle\omega^2\rangle^i, \tau_c^i) + A_w W(\omega) + C \tag{8}$$

where N indicates the number of Kubo−Anderson functions (KAF, defined by eq 5 used to describe the observed spectral features), $W(\omega)$ is the water contribution, ω_0^i is the peak wavenumber of the ith component, A_i and A_w are scaling factors, and C is a constant background. $W(\omega)$ has been explicitly measured and found to be weak, smooth, and structureless in the three spectral ranges of interest. Therefore, it can be simply subtracted without adding systematic errors within the signal-to-noise ratio of the measurements.

dx.doi.org/10.1021/jp3088594 | J. Phys. Chem. B 2012, 116, 13219−13227

As a first step, for each spectrum we have carried out a set of fits by varying N. As expected, on increasing N, χ^2 decreases up to an asymptotic value where $(\chi^2/J)^{1/2}$ coincides with the spectrum experimental noise. On the other hand, the use of many parameters in the fit function may lead to strong correlations among them, thus affecting the accuracy and the reliability of their determination. To avoid misinterpretation or constricted results, the likelihood of the fit procedure has been tested by means of correlation coefficients.

The correlation coefficient between two fit parameters Θ_i and Θ_j, with variances $\Delta\Theta_i$ and $\Delta\Theta_j$ can be expressed as

$$\rho_{ij} = \frac{\sigma_{ij}}{\sqrt{\sigma_{ii}\sigma_{jj}}}$$

where $\sigma_{ij} = \langle(\Theta_i - \Delta\Theta_i)(\Theta_j - \Delta\Theta_j)\rangle$ is the covariance matrix extracted from the fit routine, which measures the statistical errors on the best-fit parameters Θ_i and Θ_j.[37]

When ρ_{ij} is very close to +1 or −1, Θ_i and Θ_j are statistically not independent and, consequently, the χ^2 minimum value can be attained by several pairs of Θ_i and Θ_j values. Therefore, we have controlled that the ρ_{ij} values related to the fit parameters taken into consideration for our discussion is within ±0.2. In some specific cases in which ρ_{ij} exceeded ±0.2, the fit likelihood has been evaluated and explained in the text.

To better clarify this last point, we have reported in Table 1 an example of the correlation coefficient analysis performed on a spectrum analyzed in this work, specifically the ν(C═O) feature at n = 22 (22 water molecules per acetic acid molecule). In addiction to the χ^2 value, on the table are also reported the correlation coefficient between the parameters A_i of the various KAFs, labeled as p_a and p_b ($\sigma^A[p_a p_b]$) and wavenumber positions ω_i ($\sigma^\omega[p_a p_b]$). A substantially lower χ^2 value is reached when three KAFs are used. Instead, when four KAFs have been used, in spite of a similar value of χ^2 we find a strong correlation between the amplitudes of two peaks. It means that the fit likelihood is not guaranteed by using four components and therefore we must use three peaks for our data analysis process.

Table 1. χ^2 and Some Representatives Correlation Matrix Values Achieved from the Fitting Procedure Performed on the n = 22 ν(C═O) Spectrum by Using a Different Number of KAFs (Enumerated as p_1, p_2, p_3, and p_4)[a]

number of KAFs	χ^2	p_a, p_b	$\sigma^\omega[p_a p_b]$	$\sigma^A[p_a p_b]$
2	0.3257	p_1, p_2	0.228	0.205
3	0.0802	p_1, p_2	0.183	−0.256
		p_1, p_3	0.202	−0.201
		p_2, p_3	0.046	0.200
4	0.0788	p_1, p_2	−0.203	0.633
		p_1, p_3	−0.173	−0.592
		p_1, p_4	−0.660	0.261
		p_2, p_3	0.320	0.204
		p_2, p_4	0.308	−0.455
		p_3, p_4	0.712	−0.957

[a] σ^A indicates the correlations matrix elements between the amplitudes (parameter A_i of eq 8), whereas σ^ω refers to the correlation matrix elements between the maximum frequency position (parameters ω_0^i of eq 8).

RESULTS AND DISCUSSION

In Figure 1a, representative Raman spectra of ν(C−C) excitation are shown as a function of concentration (n, which is the stoichiometric ratio between water and acetic acid molecules). For n = 0 (pure acetic acid) the spectrum is asymmetric with a sharp line width. On increasing n, the line width broadens and the asymmetry reduces. These changes are more evident in the $0 < n < 1$ range, whereas for $n > 10$ the variation of peak line shape is almost negligible. This behavior can be quantitatively analyzed using the proposed fitting procedure. Results are shown in Figure 1b. In the $0 < n < 1$ range the spectrum can be decomposed into 3 KAF. The most intense one (at n = 0) has $\alpha \simeq 0.15$. The other two peaks have α equals to 1.4 and 1.0, respectively, whereas all τ_c values are close to ≃3 ps (Table 2). Because the main component has $\alpha \ll 1$, its line shape is strictly close to a Lorentzian one, with τ_{deph} = 2.9 ± 0.2 ps.

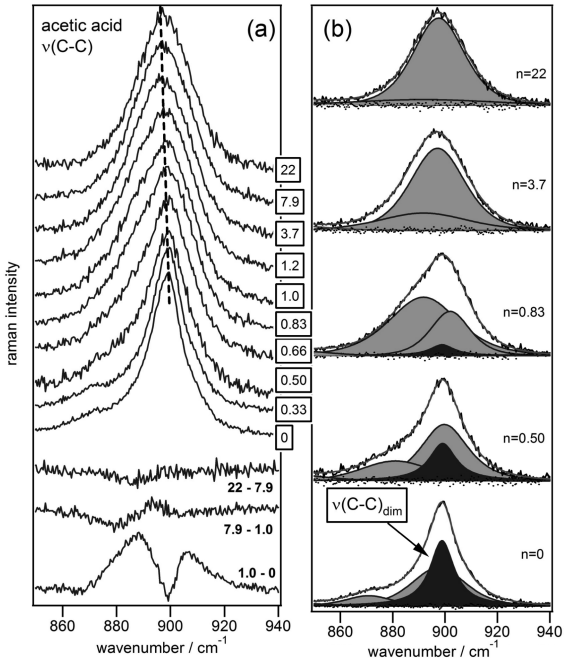

Figure 1. (a) Some representative ν(C−C) Raman peaks collected at different n values (indicated in the boxes near each curve). All the spectra have been normalized to their maximum amplitude. In the lower part of the panel is reported the difference between the spectra at some representative n values. The dotted line is a guide for the eyes evidencing the trend of the peak wavenumber. (b) Example of fitting results for some representative n values. The black shaded peak is the $\nu(C-C)_{dim}$ component.

Several works have demonstrated the presence of so-called cyclic dimers both in the liquid and in the gaseous phase of pure acetic acid;[38] the latter case is also characterized by a

Table 2. Fit Results of the ν(C−C) Pure Acetic Acid Raman Spectrum

	α	τ_c (ps)	$\langle\omega^2\rangle$ (cm^{-2})
$\nu(C-C)_{dim}$	0.16 ± 0.10	2.9 ± 0.2[a]	
$\nu(C-C)_1$	1.4 ± 0.3	3.3 ± 1.0	187 ± 8
$\nu(C-C)_2$	1.1 ± 0.2	3.0 ± 1.5	150 ± 20

[a] τ_{deph}.

dx.doi.org/10.1021/jp3088594 | J. Phys. Chem. B 2012, 116, 13219−13227

Lorenzian feature of the ν(C−C) component. Such dimers are highly stable and have weak interactions between the surrounding molecules, also because they have zero dipole moment.[23] It is therefore reasonable to expect a small α value, which reflects $\langle\omega^2\rangle$ values much smaller than $1/\tau_c$. in this limit case, it has been possible to estimate τ_{deph}, which is mainly ascribed to the collisions between the cyclic dimers and the surrounding molecules. On such grounds, we can associate this peak (the most intense for $n = 0$) with acetic acid cyclic dimers; for the sake of clarity we will refer to the cyclic dimer component of the peak as $\nu(C-C)_{dim}$, and $\nu(C-C)_1$ and $\nu(C-C)_2$ stand for the other two peaks.

The other two components include all the other acetic acid molecular conformations, from the free molecule to polar H-bonded oligomers; this is explained in further detail in the following of the manuscript. It is also important to stress how the cyclic-dimer dephasing time approaches the τ_c values found for the other two components. Such a trend is consistent with the coexistence of (stable) acetic acid cyclic dimers (dim_c structure of Figure 2) and of structures made by few (two or more) acetic acid molecules bounded together by HB involving the carboxylic groups (dim_1, dim_2, dim_3, and H_{olig} structures of Figure 2) as predicted by theoretical and experimental works.[23] Hereinafter, for simplicity of reading we will refer to these structures as H oligomers.

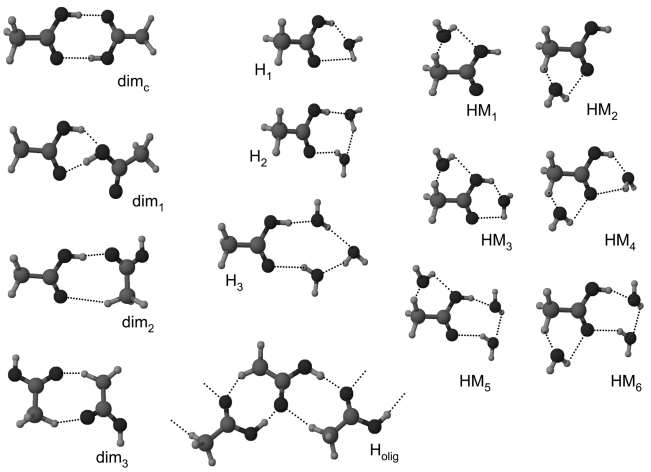

Figure 2. Schematic representation of the several HB species that can be found on acetic acid water solutions. On the left side are reported the possible dimers configurations that acetic acid may assume (dim_i). On the right side instead are reported the possible H-bonded acetic acid water structures not involving (H_i) and involving (HM_i) the methyl group. See the text for more details.

Figure 1a also evidences how the addiction of water molecules causes a strong change in the peak line shape. Qualitatively, the most relevant changes in the line shape occur within $0 < n < 1$, as shown by the difference between the spectra at $n = 1$ and $n = 0$. The fitting procedure performed on these spectra (Figure 1b) evidences a decrease in the relative intensity I^{dim}_{C-C}/I_{C-C}, being I_{C-C} the total area of the vibrational band, which vanishes for $n > 0.8$. This trend simply means that water molecules break the cyclic dimers, as known from previous results.[23]

To further confirm this interpretation, in Figure 3 we compare I^{dim}_{C-C}/I_{C-C} with the cyclic-dimer concentration calculated by Heisler and co-workers.[24] The striking agreement

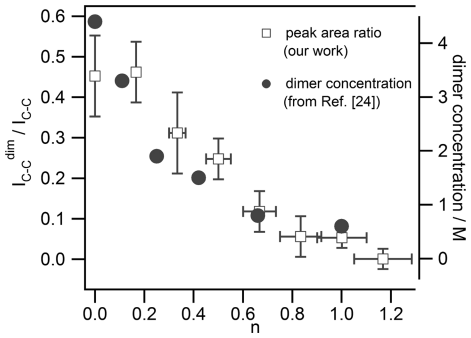

Figure 3. Relative intensity of $\nu(C-C)_{dim}$ component (open squares) as compared with the expected concentration of cyclic dimers (dots).[24]

of these trends evidence the correctness of the assumption of the disappearance of cyclic dimers at $n \approx 1$.

On increasing n above 1, the peak wavenumber difference between $\nu(C-C)_1$ and $\nu(C-C)_2$ decreases, thus leading to a noticeable reduction in the overall peak asymmetry. Moreover, the differences between the peak line shape decrease with increasing n; in particular, such changes are hardly noted for $n >$ 10.

Moreover, as the value of n increases, a progressive reduction of the fit quality occurs, as evidenced by the trend of the peak amplitudes (A_i of eq 8) correlation coefficient (Table 3).

Table 3. Correlation Coefficients (See eq 8) between the Peak Amplitudes (A_{dim}, A_1, and A_2) as a Function of n

n	$\sigma^{A_{1,2}}$	$\sigma^{A_{dim,1}}$
0	0.37	0.11
0.17	0.31	0.17
0.33	0.54	0.25
0.50	0.52	0.24
0.66	0.83	0.52
0.83	0.98	0.63
1.00	0.99	0.99

Therefore, we do not quatitatively discuss on the ν(C−C) spectra above $n = 1$. However, a qualitative consideration on the peak asymmetry can be done. Indeed, the reduction of such asymmetry on increasing n means that an overlapping of several features close in wavenumber occurs; hence suggesting that several acetic acid configurations may coexist.

The presence of several configurations is clearly evident by studying the behavior of the ν(C═O) spectra as a function of n. Such a behavior is qualitatively shown in Figure 4a. As a general feature, these spectra are more dispersed in wavenumber with respect to ν(C—C) and ν(C−H) ones, covering a wavenumber range of ≈200 cm^{-1} instead of the ≈50 cm^{-1} range of ν(C—C) and ν(C—H) spectra. Qualitatively, such a behavior evidence the presence of several different acetic acid conformations that can be assigned to the different geometrical concentration of the HB involving the C═O group, thus confirming the central role of this functional group into HB formation.

The ν(C═O) spectra of pure acetic acid has a well-defined structured line shape, reflecting the presence of several acetic acid conformations, which is further confirmed by the following data analysis. A drastic change in the peaks line shape occurs while the water quantity is increased. As observed for the ν(C—C) spectra, the most relevant changes in the line shapes

dx.doi.org/10.1021/jp3088594 | J. Phys. Chem. B 2012, 116, 13219−13227

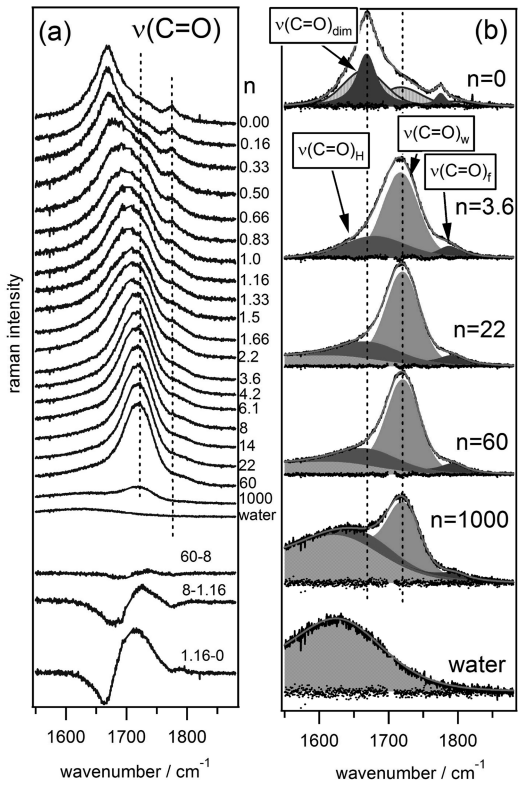

Figure 4. (a) n evolution of the line shape of ν(C═O) excitation. The numbers on the right of the curves are the corresponding n values. All the peaks are normalized to their maximum amplitude, apart from the n = 1000 and the water ones. In the lower part of the graph differences between the spectra at some representative n values are reported. Dotted lines are guides for the eyes to evidence the n trend of the main spectral features. (b). Example of fitting results of some significatives ν(C═O) spectra as a function of n (indicated in the individual sup-panels).

occur in the $0 < n < 1$ range, as also evidenced by the spectra difference reported in the bottom of Figure 4a. Between $1 < n < 10$ a line shape change is still present, although less relevant, whereas above n = 10 no significant line shape changes seems to occur.

Figure 4b shows the fitting results performed at n = 0, 3.6, 22, 60, and 1000. For n = 0, five KAF are needed to achieve a reliable fit (Table 4); two of the five components are characterized by a small α value. The most intense peak (labeled as $\nu(C{=}O)_{dim}$), at a wavenumber position of 1668 cm^{-1}, has $\alpha \simeq 0.18$ and $\tau_{deph} \simeq 2.5$ ps. This peak can be easily assigned to the C═O vibrations of the cyclic acetic acid dimers.[23] Another peak with a small α value (labeled as $\nu(C{=}O)_f$) is observed at 1775.3 ± 0.3 cm^{-1}; it can be associated with the end-chain acetic acid molecules or with the free acetic acid molecules.[23] In these cases the interactions between the surrounding molecules are expected to be fairly weak, thus explaining the small α values observed for these components.

The other three peaks instead (labeled $\nu(C{=}O)_1$, $\nu(C{=}O)_2$, and $\nu(C{=}O)_3$) have α values greater than 3 and τ_c values of about 3 ps. They can be associated with noncyclic dimers, trimers, pentamers, or longer hydrogen-bonded acetic acid chains, in agreement with previous studies performed on acetic acid liquid phase[23,24,35](see dim_1, dim_2, dim_3, and H_{olig} structures of Figure 2). Therefore, because such oligomers are characterized by HB structures, it is reasonably to assume that the estimated τ_c values match with the HB lifetime.

Remarkable variations in the peaks line shape are obserbed on increasing n, because the spectra tend to assume a less-structured line shape. For $0 < n < 3$ reliable parameters cannot be extracted from the spectra, because the minimum number of KAFs that does not lead to strong correlations between fitting parameters does not generate a small and homogeneous residual. Therefore, in this n range, we limited our considerations to an empirical line shape analysis. The difficulties in obtaining a reliable fit further confirms the large degree of disorder present of the investigated system, which can be addressed to the large number of HB geometries that the carbonyl group may adopt with the surrounding molecules.

At $n > 3.6$ a reliable fit can be again obtained by using three KAFs. The peak at 1775.3 cm^{-1}, which has been assigned to the end-chain/free acetic acid molecules, remains visible in the whole n range (dotted line in Figure 4a), while the peak wavenumber moves toward 1785 cm^{-1} on increasing n. Moreover, in all the probed n range the α value of such a peak results to be always smaller than 0.2, with a τ_{deph} ranging from 2 to 3 ps. We can then reasonably assume that, as in the case of n = 0, such a peak corresponds to the C═O groups, which do not interact with water and the other acetic acid molecules (i.e., free HB's). Hereafter we will refer to this peak as $\nu(C{=}O)_f$, whereas the further two components will be quoted as $\nu(C{=}O)_w$ (peak at ≈1725 cm^{-1}) and $\nu(C{=}O)_H$ (peak at ≈1725 cm^{-1}).

Qualitatively, from Figure 4 it can be shown how, while n increases, the $\nu(C{=}O)_w$ component becomes predominant with respect to the others. To analyze more quantitatively such a behavior, in Figure 5 is shown the relative integrated area of the three peaks ($I^w_{C=O}/I_{C=O}$, $I^H_{C=O}/I_{C=O}$ and $I^f_{C=O}/I_{C=O}$, $I_{C=O}$ being the total area of the C═O spectral band). The graph evidences how the relative intensity of the $\nu(C{=}O)_f$ component remains almost constant around ≃0.1 in the whole n range, while we observe a gradual increase of the $\nu(C{=}O)_w$ component accompanied by a consequent decrease of the $\nu(C{=}O)_H$ one. In the inset of Figure 5 the ratio of the $\nu(C{=}O)_w$ and $\nu(C{=}O)_H$ integrated spectral intensity is reported as a function of n. The graph clearly shows two different trends, below and above $n \simeq 10$. Below n = 10 $I^H_{C=O}$ decreases rapidly, evidencing strong variations in the HB conformations of the solution, whereas above n = 10 such decreasing is sensibly reduced. The raise of the $\nu(C{=}O)_w$ component by increasing n led us to suppose that this can be ascribed to dimers between water and acetic acid involving the C═O groups, or to more complex H oligomers involving water.

Table 4. Fit Results of the ν(C═O) Pure Acetic Acid Raman Spectrum (n = 0)

	peak position (cm^{-1})	α	τ_c (ps)	relative peak area (error 20%)
$\nu(C{=}O)_{dim}$	1668.22 ± 0.09	0.18 ± 0.10	2.5 ± 1.0[a]	0.34
$\nu(C{=}O)_1$	1664.67 ± 0.07	3.2 ± 0.5	2.9 ± 0.5	0.37
$\nu(C{=}O)_2$	1717.35 ± 0.15	3.2 ± 0.5	3.1 ± 0.5	0.19
$\nu(C{=}O)_3$	1789.54 ± 0.35	3.0 ± 0.5	3.3 ± 1.0	0.05
$\nu(C{=}O)_f$	1775.04 ± 0.30	0.15 ± 0.10	3.0 ± 1.5[a]	0.04

[a] τ_{deph}.

dx.doi.org/10.1021/jp3088594 | J. Phys. Chem. B 2012, 116, 13219−13227

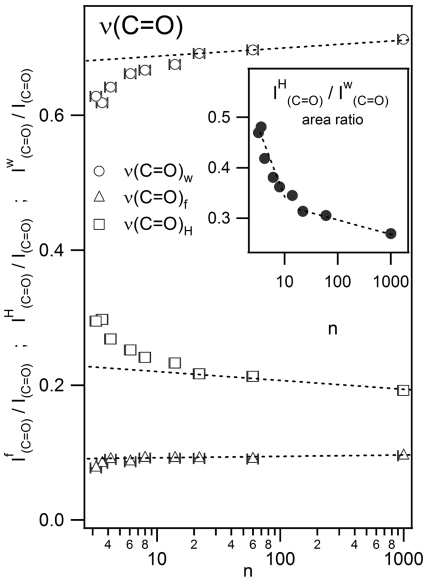

Figure 5. n dependence of $I^w_{C=O}/I_{C=O}$, $I^H_{C=O}/I_{C=O}$, and $I^f_{C=O}/I_{C=O}$ area ratios. The inset reports the $I^H_{C=O}/I^w_{C=O}$ area ratio. Dotted lines are guides for the eyes to highlight the n trend.

Further information on the nature of these peaks can be derived by analyzing the fitting results. Figure 6 shows the n

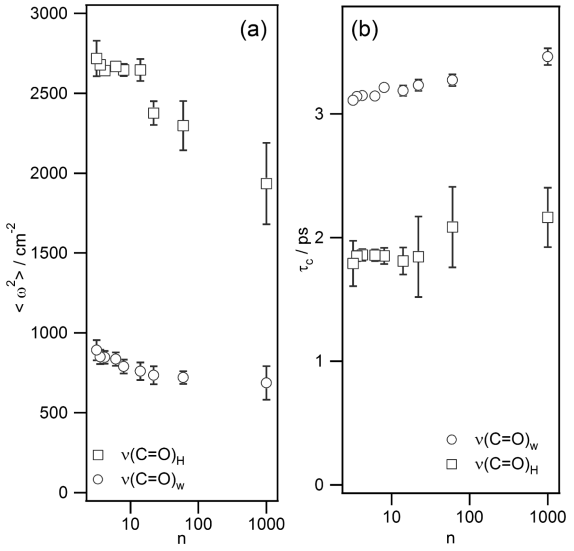

Figure 6. (a) $\langle\omega^2\rangle$ values of the $\nu(C{=}O)_w$ and $\nu(C{=}O)_H$ components as a function of n. (b) τ_c values of the of the $\nu(C{=}O)_w$ and $\nu(C{=}O)_H$ components as a function of n.

trends of $\langle\omega^2\rangle$ (panel a) and τ_c (panel b) of the $\nu(C{=}O)_H$ and $\nu(C{=}O)_w$ components. The $\nu(C{=}O)_w$ τ_c is always greater than 3 ps, whereas the $\nu(C{=}O)_H$ τ_c is below 2 ps. Moreover, the $\langle\omega^2\rangle$ trend points toward an increase of this parameter, which evidences a simplification of the C=O HB network; while the $\nu(C{=}O)_w$ component $\langle\omega^2\rangle$ becomes constant above $n \simeq 10$, $\langle\omega^2\rangle$ for the $\nu(C{=}O)_H$ component is always lower than that of $\nu(C{=}O)_w$ one. Finally, the $\langle\omega^2\rangle$ values of the $\nu(C{=}O)_H$ peak are almost constant within the experimental error in the $0 < n < 10$ range.

This higher degree in the structural disorder of the $\nu(C{=}O)_H$ component with respect to the $\nu(C{=}O)_H$ one confirms the hypothesis that the $\nu(C{=}O)_H$ peak can be mainly associated with the C=O groups involved in noncyclic dimers, trimer, pentamer, or more complex H-bonded structures (i.e., H oligomers) predicted by Nishi and co-workers (see also Figure 2).[23] Furthermore, the lower τ_c values of the $\nu(C{=}O)_H$ feature with respect to the $\nu(C{=}O)_w$ one are consistent with such attribution, because a lower binding energy is needed to create acetic acid−water structures with respect to the ones needed to create H oligomers (Table 5). On such grounds the attribution of the $\nu(C{=}O)_w$ component to the acetic acid water dimers results to be fully consistent.

Table 5. Estimated Binding Energy and $\nu(C{=}O)$ Wavenumbers for Several Acetic Acid Hydrates (from ref 35)

		wavenumber (cm^{-1})	
hydrates[a]	binding energy (kJ/mol)[a]	theor[a]	exp[b]
H_1	−35.4	1793	1720
H_2	−78.7	1781	1675
H_3	−112	1779	
HM_1	−14.3	1836	
HM_2	−21.1	1806	
HM_3	−50.4	1806	
HM_4	−56.8	1775	
HM_5	−94.4	1806	
HM_6	−99.9	1758	

[a]From ref 35. [b]Present work.

The n dependence of the peak wavenumber of the $\nu(C{=}O)$ component is shown in Figure 7. The graph evidence a smooth

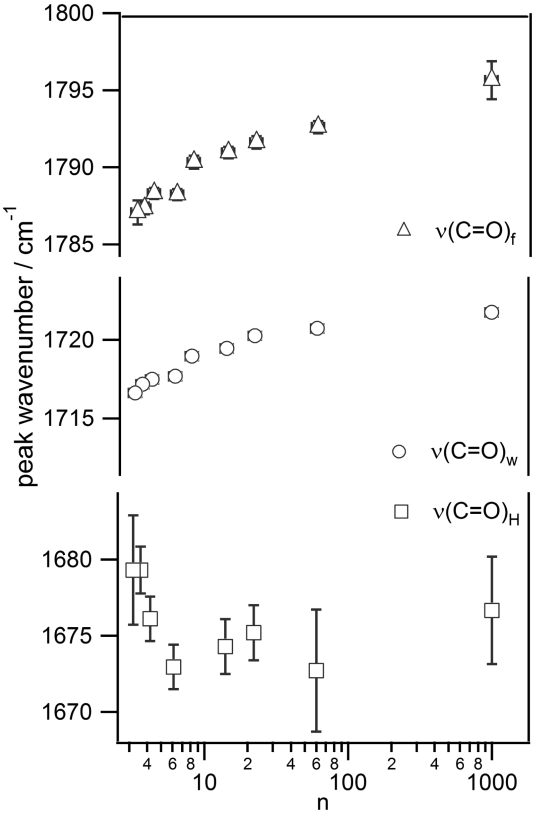

Figure 7. n dependence of the peak wavenumber of the $\nu(C{=}O)_H$ (squares), $\nu(C{=}O)_w$ (circles), and $\nu(C{=}O)_f$ (triangles) components.

dx.doi.org/10.1021/jp3088594 | J. Phys. Chem. B 2012, 116, 13219−13227

increase in the peaks wavenumber by increasing n for $\nu(C{=}O)_w$ and $\nu(C{=}O)_f$, whereas below $n = 10$ the $\nu(C{=}O)_H$ peak wavenumber decreases from 1695 to 1705 cm^{-1}. For $n > 10$, instead, the $\nu(C{=}O)_H$ wavenumber position is almost constant at a value ≈1675 cm^{-1} within the experimental error.

To account for the wavenumber change of $\nu(C{=}O)_H$ peak, we made the hypothesis that another structural acetic acid HB conformation is included in this peak, using as reference molecular dynamics simulation results by Pu and co-workers.[35] Table 5 shows the calculated binding energies and vibrational frequencies for the H-bonded structures depicted in Figure 2. Although the reported wavenumber values are greater than the experimental ones, a wavenumber spread of ≈10 cm^{-1} between the simplest water-bonded dimer structure (H_1) and the other ones (H_2 and H_3) is expected. It must be also noted how H_1, H_2, and H_3 are more energetically favored with respect to the HM's, which involves also HB with methyl groups. This is a key aspect; indeed, it has been widely demonstrates how hydrophobic groups in aqueous solution may lead to a strong hydration shell having a local structural conformation different from that of the bulk water (see, e.g., ref 39 and references therein). Therefore, we can expect that, in very diluted solutions, the HM structures are absent because of the presence of such a strong hydration shell, thus validating the assumption that (at least in diluted solutions) the $\nu(C{=}O)_w$ component may be associated with the H_1 structure and $\nu(C{=}O)_H$, for $n >$ 10, can be associated with H_2, H_3, or more complicated structures. The behavior of $I^H_{C=O}/I^w_{C=O}$ (Figure 5) endorses such an assumption because the drastic change of the n trend at $n \simeq 10$ may represent the n point in which the H oligomers disappear and acetic acid can only forms HB with water molecules.

To better take into account the behavior of such H oligomers in the $1 < n < 10$ range, in particular those in which the HB involve the methyl groups, we have considered the fit results achieved from the $\nu(C{-}H)$ spectra. The $\nu(C{-}H)$ vibrational peak, visible in the range 2900−3000 cm^{-1}, can be modeled by a single KAF in all the exploited n range (Figure 8a). In this small energy range the spectrum is dominated by the symmetric $\nu(C{-}H)$ stretching, referred to in the following as $\nu_s(C{-}H)$. The presence of a single component is consistent with the very small energy shifts associated with the several possible acetic acid conformations, which, indeed, are estimated to be ≃1−2 cm^{-1}.[35]

The peak wavenumber for this feature is shown in Figure 8b as a function of n. It was found to follow a smooth n increase, characterized by three distinct trends. For both $n < 0.8$ and $n >$ 20 the rate of the n increase is substantially lower than that found in the 1−10 n range. These n ranges fairly match the changes observed at $n \approx 1$ and at $n \approx 10$ in the trends of $\nu(C{—}C)$ and $\nu(C{=}O)$.

Further information can be gained by analyzing the α-behavior as a function of n (shown in Figure 8c): α has initially a rapid rise with increasing n; such a rise becomes less intense whereas n increases until an almost constant value at high n.

Although with $\alpha \simeq 0.1$ it is not possible to discriminate $\langle\omega^2\rangle$ and τ_c from the fit (the two parameters are strictly correlated) we can still try to analyze their behavior through the information derived from the analysis of the $\nu(C{—}C)$ and $\nu(C{=}O)$ spectra.

The rise in the α value can be attributed to an increase in τ_c or $\langle\omega^2\rangle$ (or both). Because the information coming from the $\nu(C{—}C)$ and $\nu(C{=}O)$ spectra indicates a simplification of the

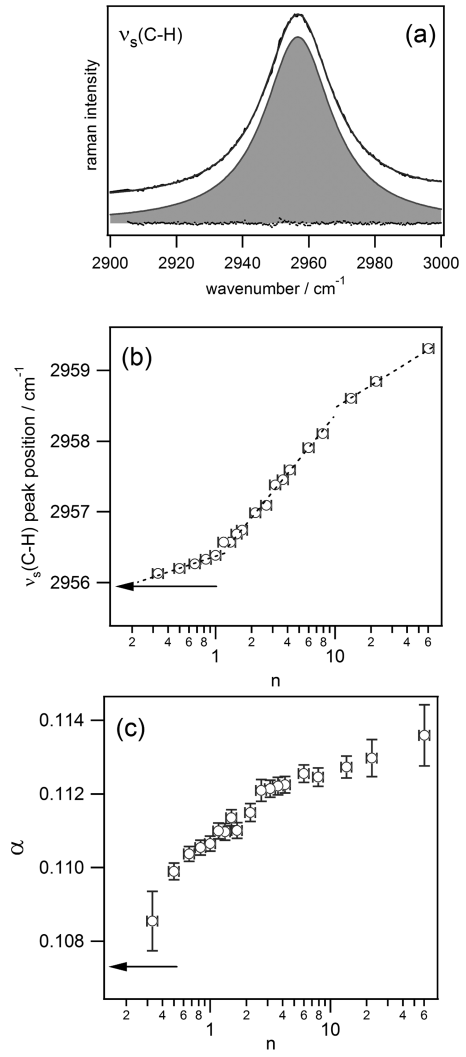

Figure 8. (a) Example of fitting result of pure acetic acid spectrum (n = 0). (b) Peak wavenumber of $\nu_s(C{-}H)$ Raman feature as a function of n. The arrow represents the peak position at n = 0 (pure acetic acid). Dashed lines are guides for the eyes. (c) α value of the $\nu_s(C{-}H)$ component as a function of n. The arrow represents the α position at n = 0 (pure acetic acid).

HB structures, it seems to be counterintuitive to expect a rise in $\langle\omega^2\rangle$. Therefore, we can reasonably suppose that the α rise reflects a τ_c increase vs n. Because we expect, as seen in the $\nu(C{=}O)$ peak analysis, a higher τ_c value for the hydrated structures with respect to the others (H oligomers), we can then assert that the τ_c increase is due to a reduction of such H oligomers (forming HB between methyl and carboxylic groups), which are progressively broken by the addition of water.

It is noteworthy to observe how the most relevant change in peak position and in α occurs in the $1 < n < 10$ range. This trend can be explained in terms of the disruption of the HB between the methyl and the carboxylic groups of acetic acid, which drastically changes the local environment felt by the vibrating atoms in the methyl group. For $n > 10$, instead, no important variations seem to occur in both peak position and α.

The observed discontinuities in peak parameters and the smaller variations occurring in all peaks for $n > 10$ led us to suppose that $n \approx 10$ is the limit above of that the hydration shell around the methyl group is completed, and therefore,

dx.doi.org/10.1021/jp3088594 | J. Phys. Chem. B 2012, 116, 13219−13227

further addition of water turns only in an increase of bulk water content. The presence of such an hydrophobic shell is also endorsed by the high and almost constant α value at $n > 10$ with respect to the α values at $n < 10$, which reflects (as explained above) a higher and constant τ_c value at $n > 10$. The n range between 1 and 10 can be therefore considered as the transition region where the H oligomer structures are gradually broken in favor of the formation of dimer structures, like H_1, H_2, and H_3. The last two structures, although less intense with respect to H_1, are present also in diluted solutions, whereas the hydrophobic core surrounding the methyl groups may avoid the formations of HM structures.

SUMMARY AND CONCLUSIONS

The line shape analysis for all the three acetic acid vibration peaks presented in this paper evidence the presence of three distinct n regions in acetic acid aqueous solutions.

In the first region ($0 < n < 1$) the solution presents the most relevant changes in structural conformations. At $n = 0$ (pure acetic acid) the spectra show, as expected, the leading presence of acetic acid cyclic dimers, similar to the ones observed in the gas phase. The cyclic dimers coexist, as supposed by several authors,[23−25] with H-bonded acetic acid dimers, trimers, pentamers, or larger H-bonded oligomers chains, thus leading to a relevant structural disorder. The small α value for the Kubo−Anderson Raman features associated with cyclic dimers mirrors negligible interactions between these dimers and the other H-bonded acetic acid chains. When n increases from 0 to 1, the large variations in the ν(C═O) and ν(C—C) line shapes are the proof of a radical change in the liquid structural conformation. The addition of (polar) water molecules breaks the (apolar) acetic acid cyclic dimers, favoring the formation of acetic acid water dimers; the H-bonded oligomers also involve the acetic acid methyl group. This is fully consistent with computational results, which predict the existence of H-bonded acetic acid oligomer structures involving HB's between carboxylic and methyl groups.

Between $n = 2$ and $n = 10$ the spectral behavior evidences the progressive breaking of H-bonded oligomers favoring the formation of acetic acid water dimers. This breaking principally involves the HB between the acetic acid methyl groups and the carboxylic ones, i.e., the links of H oligomer chains. The observed τ_c increase vs n in the ν(C═O) components involving water−acetic acid dimers highlights a certain rigidity of the HB between water and the carbonyl group of acetic acid. This process, indeed, leads to the reduction of the H oligomers presence and, consequently, favors the generation of an hydration shell surrounding acetic acid.

At $n \simeq 10$ the acetic acid hydration shell is completed. Further addiction of water molecules does not significantly modify the spectral line shape, thus confirming that the HB structure between water and acetic acid are stabilized and the addiction of further water molecules only leads to an increase in bulk-water content. In this case the HB between water and acetic acid does involve methyl groups, because the hydrophobic shell around the methyl groups is completed.

The agreement of the present results, achieved through a Raman line shape analysis, with previous computational and experimental data obtained with other techniques confirms the correctness of using the Kubo−Anderson model to study the behavior of organic solutions. We also remark how the proposed data analysis strategy could be profitably used in combination with a more selective technique, such as resonant Raman. In summary, the proposed approach can likely help in understanding the structural and dynamic behavior of organic solutions of biological interest even where complicated systems (e.g., polymers or proteins) are considered.

AUTHOR INFORMATION

Corresponding Author

*E-mail: francesco.damico@elettra.trieste.it.

Notes

The authors declare no competing financial interest.

ACKNOWLEDGMENTS

The authors acknowledge support from the European Research Council through the ERC Grant N.202804-TIMER.

REFERENCES

(1) Baker, E. N.; Hubbard, R. E. *Prog. Biophys. Mol. Biol.* **1984**, *44*, 97−179.
(2) Sheu, S.; Yang, D.; Selzle, H.; Schlag, W. *Proc. Natl. Acad. Sci. U. S. A.* **2003**, *100*, 12683−12687.
(3) Pace, C. *Nat. Struct. Mol. Biol.* **2009**, *16*, 681−682.
(4) Shirota, H.; Ushiyama, H. *J. Phys. Chem. B* **2008**, *112*, 13542−13551.
(5) Klotz, I. *Protein Sci.* **1993**, *2*, 1992−1999.
(6) Chaplin, M. *Nat. Rev. Mol. Cell Biol.* **2006**, *7*, 861−866.
(7) Ball, P. *Chem. Phys. Chem.* **2008**, *9*, 2677−2685.
(8) Bellissent-Funel, M. *J. Mol. Liq.* **2000**, *84*, 39−45.
(9) Mattos, C. *J. Mol. Liq.* **2002**, *27*, 203−208.
(10) Gao, J.; Bosco, D. A.; Powers, E. T.; Kelly, J. W. *Nat. Struct. Mol. Biol.* **2009**, *16*, 684−690.
(11) Dill, K. A. *Biochemistry* **1990**, *29*, 7133−7155.
(12) Ferraro, J. R.; Nakamoto, K.; Brown, C. W. *Introductory Raman Spectroscopy*, 2nd ed.; Elsevier: Amsterdam, 2003.
(13) Asher, S. A. *Anal. Chem.* **1993**, *65*, 59A−66A.
(14) Asher, S. A. *Anal. Chem.* **1993**, *65*, 201A−210A.
(15) Campbell, J. H.; Fisher, J. F.; Jonas, J. *J. Chem. Phys.* **1974**, *61*, 346−360.
(16) Bischel, W. K.; Dyer, M. J. *Phys. Rev. A* **1986**, *33*, 3113−3123.
(17) Nara, M.; Sakamoto, A.; Yamamichi, J.; Tasumi, M. *Biopolymers* **2001**, *62*, 168.
(18) Schlamadinger, D. E.; Gable, J. E.; Kim, J. E. *J. Phys. Chem. B* **2009**, *113*, 14769.
(19) Hédoux, A.; Ionov, R.; Willart, J.; Lerbret, A.; Affouard, F.; Guinet, Y.; Descamps, M.; Prévost, D.; Paccou, L.; Danéde, F. *J. Chem. Phys.* **2006**, *124*, 014703.
(20) Woodruff, W. H.; Norton, K. A.; Swanson, B. I.; Fry, H. A. *Proc. Natl. Acad. Sci. U. S. A.* **1984**, *81*, 1263−1267.
(21) Movileanu, L.; Benevides, J. M.; Thomas, G. J. *J. Raman Spectrosc.* **1999**, *30*, 637−649.
(22) Movileanu, L.; Benevides, J. M.; Thomas., G. J. *Biopolymers* **2002**, *63*, 181−194.
(23) Nishi, N.; Nakabayashi, T.; Kosugi, K. *J. Phys. Chem. A* **1999**, *103*, 10851−10858.
(24) Heisler, I. A.; Mazur, K.; Yamaguchi, S.; Tominaga, K.; Meech, S. R. *Phys. Chem. Chem. Phys.* **2011**, *13*, 15573.
(25) Nakabayashi, T.; Kosugi, K.; Nishi, N. *J. Phys. Chem. A* **1999**, *103*, 8593−8603.
(26) Rothschild, W. G. *J. Chem. Phys.* **1976**, *65*, 455−462.
(27) Nafie, L. A.; Peticolas, W. L. *J. Chem. Phys.* **1972**, *57*, 3145−3155.
(28) Kubo, R. *Fluctuation, Relaxation and Resonance in Magnetic Systems*; D. Ter Haar Oliver and Boyd: Edinburgh, 1962; p 27.
(29) Kubo, R. *J. Phys. Soc. Jpn.* **1962**, *17*, 1100.
(30) Mariani, L.; Morresi, A.; Cataliotti, R. S.; Giorgini, M. G. *J. Chem. Phys.* **1996**, *104*, 914−922.
(31) Marri, E.; Morresi, A.; Paliani, G.; Cataliotti, R. S.; Giorgini, M. G. *Chem. Phys.* **1999**, *243*, 323−332.

(32) Morresi, A.; Sassi, P.; Ombelli, M.; Cataliotti, R. S.; Paliani, G. *J. Raman Spectrosc.* **2000**, *31*, 577.
(33) Ombrelli, M.; Morresi, A.; Sassi, P.; Paliani, G. *J. Mol. Liq.* **2002**, *96*, 379.
(34) Edsall, J. *J. Chem. Phys.* **1936**, *4*, 1−8.
(35) Pu, L.; Sun, Y.; Zhang, Z. *J. Phys. Chem. A* **2010**, *114*, 10842.
(36) D'Amico, F.; Bencivenga, F.; Gessini, A.; Masciovecchio, C. *J. Phys. Chem. B* **2010**, *114*, 10628−10633.
(37) Nakamura, K. *J. Phys. G: Nucl. Part. Phys.* **2010**, *37*, 346−370.
(38) Bertie, J.; Michaelian, K. *J. Chem. Phys.* **1982**, *77*, 5267−5271.
(39) Petersen, C.; Tielrooij, K. J.; Bakker, H. J. *J. Chem. Phys.* **2009**, *130*, 214511.